Acta Geotechnica (2022) 17:2697–2710
https://doi.org/10.1007/s11440-021-01403-6

RESEARCH PAPER

Microscopic origin of shape-dependent shear strength of granular materials: a granular dynamics perspective

Yuxiong Zou[1,2] · Gang Ma[1,2] · Jiangzhou Mei[1,2] · Jidong Zhao[3] · Wei Zhou[1,2]

Received: 21 July 2021 / Accepted: 13 October 2021 / Published online: 9 November 2021
© The Author(s), under exclusive licence to Springer-Verlag GmbH Germany, part of Springer Nature 2021

Abstract
The shear strength of granular materials has been found to increase nonlinearly with particle asphericity before reaching a steady value independent of particle asphericity. Although the origin of shear strength has been extensively studied, the underlying mechanism of its nonlinear dependency on particle shape remains unclear. In this study, we present a microscopic investigation of shape-dependent shear strength from the perspective of particle dynamics. A series of numerical simple shear tests on assemblies of ellipsoids with different aspect ratios are performed using the discrete element method. It is confirmed that the power-law scaling in nonlocal granular rheology is still valid for granular materials composed of non-spherical particles, such that the macroscopic shear strength and microscopic dynamics can be bridged using granular temperature. Analogous to other amorphous solids, granular materials with higher granular temperature are much softer and exhibiting less resistance to shear. The statistics of the clusters of the particles with higher granular temperature indicate that granular systems with different particle shapes showing different collective motion patterns. We further explore the coupling between rotational and translational particle dynamics and their long-range correlations. The macroscopic shear strength shows a clear monotonic relation with the intrinsic length scale reflecting long-range dynamic correlations. Finally, we propose a picture illustrating the negative feedback mechanism between particle rolling and sliding, which leads to the nonlinear increase and steady value of shear strength with particle asphericity. Our finding may shed light not only on the particle shape effects, but also on the fundamental understanding of the microscopic origin of shear strength of granular materials.

Keywords Granular materials · Granular temperature · Microscopic dynamics · Particle shape · Shear strength · Spatial correlation

1 Introduction

Granular materials refer to a class of natural and man-made materials consisting of individual particles, featuring inhomogeneous, anisotropic, and disordered internal structures. In different circumstances, granular materials exhibit complex physical properties and mechanical behaviors [28, 30]. The complicated behavior of granular media on the macroscopic level is known to be closely related to the complexity of their underlying microstructure [72]. The particle-scale properties, such as particle shape [4, 12, 34, 40, 68, 69, 74, 77], surface friction [8, 17, 55] and size polydispersity [25, 49, 78], contribute significantly to the mechanical behaviors at the ensemble level. This is attributed to the multiscale nature of granular materials, where complex macroscopic responses emerge from particle interactions and particle dynamics. In spite of great efforts, it remains a challenge to directly relate the microscopic behaviors to the macroscopic responses to render rigorous cross-scale understandings [73].

Particle shape is regarded as one of the most important particle-scale characteristics, which significantly affects the

✉ Gang Ma
magang630@whu.edu.cn

1 State Key Laboratory of Water Resources and Hydropower Engineering Science, Wuhan University, Wuhan 430072, China

2 Key Laboratory of Rock Mechanics in Hydraulic Structural Engineering of Ministry of Education, Wuhan University, Wuhan 430072, China

3 Department of Civil and Environmental Engineering, The Hong Kong University of Science and Technology, Clear Water Bay, Kowloon, Hong Kong, China

macroscopic behaviors of granular materials, such as shear strength [60, 62, 69], packing density [14, 16, 51, 59], dilatancy [3, 67], and plastic deformation [50]. Among the various mechanical properties affected by particle shape, the shear strength has attracted much attention for its importance in industry and engineering applications. Extensive experimental studies have reported that the shear strength increases with particle asphericity [34, 60, 62, 69]. The most commonly accepted explanation is that irregular particle shape suppresses particle rotation and thus enhances the particle inter-locking effects, which results in the increase of shear strength [34, 62, 76]. Using particle-based numerical simulation methods, some studies have further found that the shear strength has a curvilinear relation with particle asphericity [4, 5, 10, 26, 58]. Specifically, the shear strength increases with asphericity up to a maximum value, and further increase the particle asphericity will not improve the shear strength.

Microscopic investigations from different perspectives have been dedicated to gain a full understanding of the nonlinear shape dependence of shear strength. For example, due to the enhanced arching effect, the proportion of weak contact increases with particle asphericity [5, 6]. Focuses of many other studies are placed on the effects of particle shape on the anisotropy of different sources in granular materials, such as fabric anisotropy and mechanical anisotropy. The well-developed stress-force-fabric (SFF) relationship enables the stress ratio to be expressed in terms of different anisotropic coefficients [52, 71]. As such, the effects of particle shape on shear strength can be quantified based on anisotropy analysis. It is generally accepted that both the fabric anisotropy and contact force anisotropy are enhanced by particle asphericity [10, 71, 74]. For angular particles, the increase of the shear strength with angularity mainly results from the increase of contact force anisotropy [6, 74]. For elongated particles, the increase of the shear strength with aspect ratio is attributed to the combined effect of fabric anisotropy and contact force anisotropy, which may result from the formation of an ordered nematic phase in which the particle axes align along a common direction [5, 10, 26, 71]. The contribution of different sources of anisotropy to shear strength varies from case to case. Therefore, we still need a more fundamental explanation for the particle shape dependence of shear strength, especially the underlying mechanism responsible for the saturation of shear strength.

There is also a growing interest in investigating the granular dynamics to offer new insights into the emergent behaviors of granular materials [2, 17, 38, 39, 43, 46]. Compared with the fabric structure and force transmission, the particle dynamics of granular materials can be more easily obtained from experimental observations and numerical simulations. Recent studies have revealed the effective macroscopic fluidity is controlled by velocity fluctuations of particles, suggesting that the shear flow of granular materials is strongly dependent on the particle scale dynamics [23, 35]. In this study, we present an investigation of this long-lasting puzzle in granular materials from the perspective of particle dynamics. We first confirm that the recently developed power-law scaling in nonlocal granular rheology is still valid for non-spherical granular systems [35]. We then probe the particle dynamics of granular systems composed of particles of different shapes and systematically investigate their long-range correlations. A relationship between shear strength and the intrinsic length scale reflective of long-range dynamic correlations is established. For a plain interpretation, we finally explain the influence of particle shape based on two microscopic dynamic events of rolling and sliding.

2 Model and simulation details

2.1 Brief introduction of computational methods of discontinua

Nowadays, computational techniques, e.g., the discrete element method (DEM), are increasingly popular in various domains of science and engineering on capturing the mechanical behaviors of granular materials while providing grain-scale insights. In DEM, the translation and rotation of the particles are governed by the following Newton–Euler equations:

$$\begin{cases} \mathbf{F}^{(b)} + \sum_{k=1}^{N_c} \mathbf{F}_k^{(c)} = m\dfrac{d\mathbf{v}}{dt} \\ \sum_{k=1}^{N_c} \mathbf{M}_k^{(c)} = \mathbf{I}\dfrac{d\boldsymbol{\omega}}{dt} \end{cases} \tag{1}$$

where m is particle mass; $\mathbf{I}$ is the moment of inertia of the particle;$\mathbf{v}$ and $\boldsymbol{\omega}$ are the translational and angular velocities; $\mathbf{F}^{(b)}$ is the body force; $\mathbf{F}_k^{(c)}$ is the contact force at contact k; $\mathbf{M}_k^{(c)}$ is the torque around the mass center at contact k; and N_c is the number of contacts. In the soft-particle DEM, particles are allowed to overlap, and the contact forces are calculated as functions of the overlap as follows:

$$\begin{cases} F_n = k_n\delta_n - \gamma_n v_n \\ F_t = \min\{k_t\delta_t - \gamma_t v_t, \mu_p F_n\} \end{cases} \tag{2}$$

where k_n and k_t are the normal and tangential contact stiffness which are determined by the overlap, particle radius, Young's modulus, and Poisson's ratio in the Hertz-Mindlin contact model [32]; δ_n is the normal overlap distance; δ_t is the tangential displacement between two particles for the duration of the time they are in contact; γ_n and

γ_t are viscoelastic damping constant for normal contact and tangential contact; v_n and v_t are normal and tangential component of the relative velocity; μ_p is coefficient of friction.

In addition to DEM, the combined finite and discrete element method (FDEM) is also a popular numerical approach due to its great advantages not only in considering the irregular particle shapes but also in particle breakage [22, 41–45]. In FDEM analysis framework, each particle with arbitrary shape is discretized into finite element meshes, and the deformation of individual particles is simulated using the FEM formulation, while DEM techniques handle the contact detection and interaction. The advantage of FDEM in the modeling of non-spherical particles is obvious; however, FDEM generally requires considerable computational resources and thus not feasible for simulations of a large number of particles. For that reason, DEM is applied as a tool to probe the behavior of granular systems in this work.

2.2 Implementation of ellipsoidal particles in DEM

Barrett quantifies the particle shape into three aspects: form, roundness and surface texture [7]. An overly complex distortion of particle shape may not be conducive to quantifying the impact of particle shape, so we focus on the form in this work, and the ellipsoidal particle system is selected as the research object. Ellipsoid is the simple yet practical realization of non-spherical particles and can be easily incorporated into DEM. The major challenge in DEM modeling of ellipsoids is the implementation of an efficient and robust contact detection algorithm. A brief introduction of the contact detection algorithm of ellipsoids is given here, and the interested reader is referred to [53] for more details. The surface function of an ellipsoid is as follows:

$$f(\mathbf{x}) \equiv \left(\frac{x}{a}\right)^2 + \left(\frac{y}{b}\right)^2 + \left(\frac{z}{c}\right)^2 - 1 = 0 \qquad \mathbf{x} = (x, y, z)^T \tag{3}$$

where a, b, c are the half-lengths of the particles along its principal axes. $f(\mathbf{x})$ is referred as the shape function in the local (canonical) coordinate system.

Through rotation and translation operations, we can transform $f(\mathbf{x})$ to the global coordinate system and rename it as $F(\mathbf{X})$. In DEM, two contacting particles are allowed to overlap but without deformation, so the contact detection task can be converted to an optimization problem. Assuming the shape functions of two ellipsoids in the global frame are $F_1(\mathbf{X})$ and $F_2(\mathbf{X})$, the potential contact point $\mathbf{X_0}$ can be determined by solving the following optimization problem:

$$\begin{cases} F_1(\mathbf{X_0}) + F_2(\mathbf{X_0}) = \min(F_1(\mathbf{X}) + F_2(\mathbf{X})) \\ F_1(\mathbf{X_0}) = F_2(\mathbf{X_0}) \end{cases} \tag{4}$$

For the contact point $\mathbf{X_0}$ ($\mathbf{X_0}$ is inside the two ellipsoids) being determined, constraints $F_1(\mathbf{X_0}) < 0$ and $F_2(\mathbf{X_0}) < 0$ are both satisfied; thus, the contact between two particles occurs at $\mathbf{X_0}$. The contact direction is taken as the normal direction of $F_1(\mathbf{X}) = F_1(\mathbf{X}_0)$ (or $F_2(\mathbf{X}) = F_2(\mathbf{X}_0)$) at the contact point $\mathbf{X_0}$, i.e., $\mathbf{n}_{12} = \mathbf{X}_1 - \mathbf{X}_0/|\mathbf{X}_1 - \mathbf{X}_0|$ (or $\mathbf{n}_{12} = \mathbf{X}_0 - \mathbf{X}_2/|\mathbf{X}_2 - \mathbf{X}_0|$), and the normal overlap vector is $\mathbf{X}_1 - \mathbf{X}_2$ (referring to Fig. 1). The equivalent radius is calculated based on the Gaussian curvature radius at the contact point. The modified Hertz-Mindlin contact model with Coulomb sliding friction is employed to calculate the normal and tangential contact forces of ellipsoidal particles in this work [53]. Particle motion is governed by Newton–Euler equations that do not need to be adjusted for the ellipsoidal particle.

2.3 DEM simulation of simple shear

The numerical simulations were performed using LIGGGHTS, an open-source discrete element code that has been well validated and verified [36]. The simulation parameters are determined based on the mechanical properties of polyvinyl chloride (PVC) [39]. The particles have a density of 1,270 kg/m^3, Poisson's ratio of 0.38, Young's modulus of 4.1 GPa, friction coefficient of 0.4, and restitution coefficient of 0.9. For a prolate ellipsoid, the aspect ratio (AR) is defined as the ratio of major axis to minor axis (Fig. 2a). The particle size is defined as the diameter of a sphere with the same volume. The particle size is uniformly distributed between 0.9 and 1.1 $\overline{d}$ to prevent crystallization ($\overline{d}$ = 11.5 mm is the mean particle diameter). Seven assemblies of ellipsoid-shaped particles with AR of

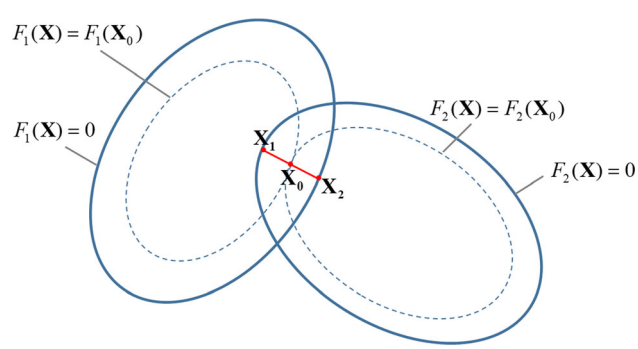

Fig. 1 Schematic of two contacting ellipsoidal particles showing the controlling variables of the overlap. The overlap is magnified for clarity

1.0, 1.25, 1.50, 1.75, 2.0, 2.5, 3.0 are prepared and used in the DEM simulations.

The model setup is shown in Fig. 2b, in which a rectangular solid domain is employed, filled with up to 50,000 particles. The sizes in the three directions are, respectively, 52 $\overline{d}$ (length) × 26 $\overline{d}$ (depth) × 30 $\overline{d}$ (height). Two rough particle walls are placed at the top and bottom of the sample to transfer shear displacements. Periodic boundaries are applied in the shear and depth directions (x-axis and y-axis). The particle assemblies are first compressed to a prescribed normal pressure P = 100 kPa. The top and bottom walls are displaced horizontally in opposite directions with a fixed velocity, while the normal pressure is maintained constant by servo-control [46, 47, 65]. The shear rate, defined as the ratio of shear velocity to the undeformed sample height, is set to $\dot{\gamma} = 0.5$. The inertia number $I = \dot{\gamma}\overline{d}/\sqrt{P/\rho_s} < 10^{-3}$ (ρ_s is the particle density) is small enough to guarantee a quasi-static regime (Midi, 2004).

Figure 2c, d shows the spatial maps of horizontal velocity v_x for two particle assemblies (AR = 1.0 and 2.0). We also compute the vertical profile of horizontally averaged particle velocity v_x. When the boundaries of a granular system are slowly sheared, a narrow shear band with a typical width of a few particle diameters emerges and develops at the sample center. The particle shape has apparent effects on the localized deformation pattern. The granular system with larger particle AR has a more distinct shear band along the shear direction, which is confirmed by the sharp transition of the velocity profile (Fig. 2d). The kink at the center of the velocity profile corresponds to the localized granular flow.

2.4 Particle shape dependence of shear strength

To generate enough data for analysis, we shear the granular systems up to a shear strain of $\gamma = 8.0$. The stress–strain curves of granular materials are illustrated in Fig. 3a. The overall response shows an overshoot behavior followed by a series of stress drops and convergence to a relatively constant value at a large strain. When the shear stress fluctuates around a mean value, it can be considered that the granular system has reached the steady state, where the memory of the initial state is fully erased. The following analyses are based on the average over the last 25% of shear strain (i.e., γ from 6.0 to 8.0). The shear strength is

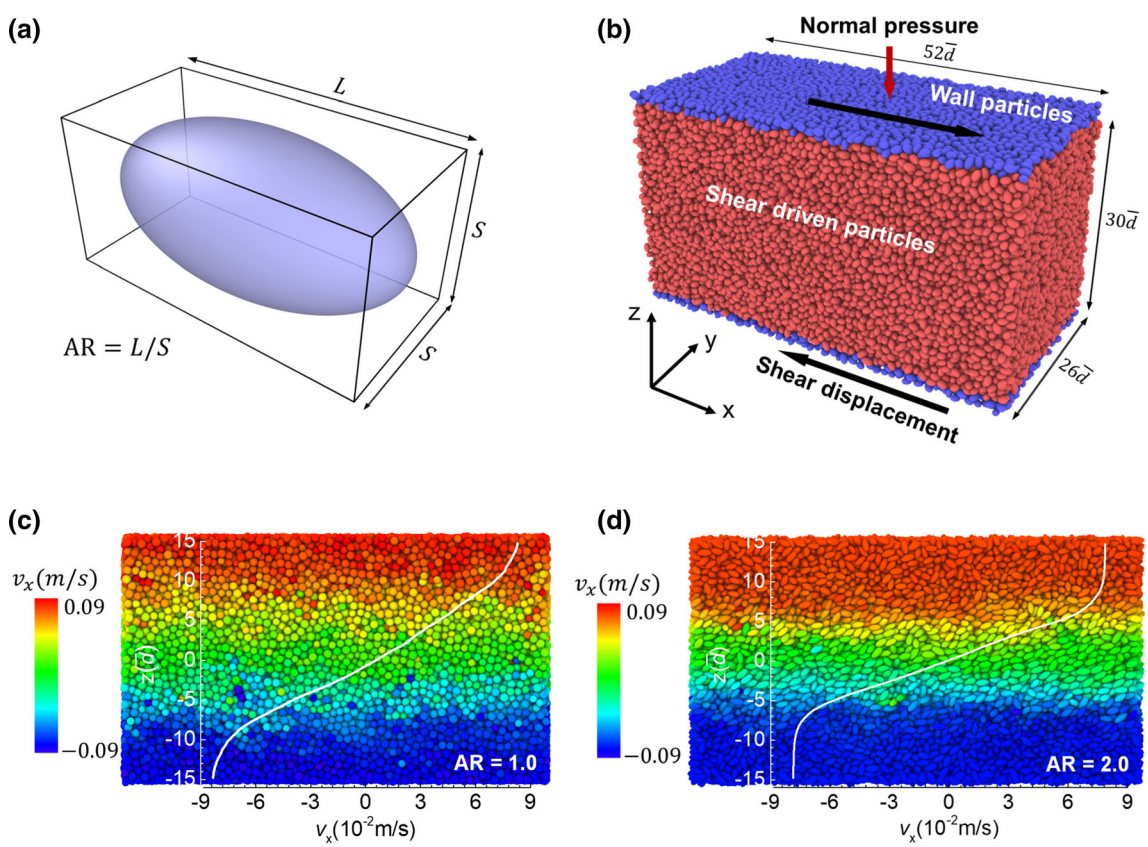

Fig. 2 **a** Definition of the aspect ratio for a prolate ellipsoid. **b** Schematic of the particle assembly and the simple shear setup. **c, d** The spatial maps of horizontal velocity v_x for granular systems with particle AR = 1.0 (spherical particle) and AR = 2.0. The white line is the profile of horizontal velocity v_x

expressed in terms of the ratio of shear stress to normal pressure. Figure 3b shows the relations between the stress ratio at steady state and particle AR. The shear strength increases nonlinearly with particle AR up to a maximum value and the increase rate slows down gradually for larger ARs. The fitting curves appear to indicate that shear strength saturates as the particles become more aspheric. The nonlinear particle shape dependence of shear strength has also been observed in granular materials made of other particle shapes, such as Rounded-cap rectangle [5], 3D square plate [10], and multi-sphere ellipsoid [26].

3 Microscopic dynamics

3.1 The relationship of stress ratio and granular temperature

Like other amorphous materials, almost all particles in the granular system are moving under shear. The shear resistance is originated from the balance between microscopic elementary rearrangements occurring in opposite directions [23]. The shear strength represents a bulk property resulting from a collective process, which depends on the nature of particle interactions and their geometrical arrangement [20]. For example, the rearrangement of irregularly shaped particles will be more limited due to inter-locking effects, exhibiting stronger resistance to shear compared to spheres. Therefore, exploring particle dynamics may be helpful to understand the nonlinear shape dependence of shear strength. In granular rheology, attempts have been made to develop nonlocal constitutive relation, which connects the global stress ratio and nonlocal fluidity [23, 33, 54]. Kim and Kamrin [35] recently proposed a general constitutive equation $\mu\Theta^{1/6} = f(I)$ that relates three dimensionless variables: stress ratio μ, inertia number I, and granular temperature Θ. The dimensionless granular temperature is defined as $\Theta \equiv \rho_s T/P$, where $T = \delta v^2/3$ and δv is the velocity fluctuation.

We layered the granular system along the z-axis and calculated μ, I, and Θ of each layer following the procedures used by Kim and Kamrin [35]. The relations between $\mu\Theta^{1/6}$ and I for granular systems with different particle shapes are shown in Fig. 4a. To verify the universality of the nonlocal constitutive relation, the data points obtained from simple shear tests of different shear rates ($\dot{\gamma}$ = 2, 5, 20) are also added into Fig. 4a. Strikingly, all the data points collapse to a single master curve in spite of different particle shapes and different shear rates used. This result indicates that the new-form nonlocal constitutive equation is independent of packing fraction, shear rate, and particle shape. As the nonlocal constitutive relation appears robust to varying particle properties in granular materials, we can use this relation to link the macroscopic response and particle dynamics of granular materials. We further examine the whole granular systems. Since the inertial number of granular systems with different particle shapes are the same in this study, the $\mu(\Theta, I)$ relation can be reduced to $\mu = g(\Theta)$. As shown in Fig. 4b, we can observe a linear relationship between μ and $1/\Theta$ in a semi-logarithmic scale. Similar to a thermal system, granular materials with higher granular temperature are softer and exhibit less resistance to shear [9]. From this point of view, the relation between shear strength and particle AR is controlled by granular temperature.

3.2 Spatial correlation of local granular temperature

The universality of nonlocal constitutive relation indicates that granular temperature plays a crucial role in mobilizing the shear strength of granular materials. We can analyze the local granular temperature to gain microscopic insight into the effects of particle shape on shear strength. The

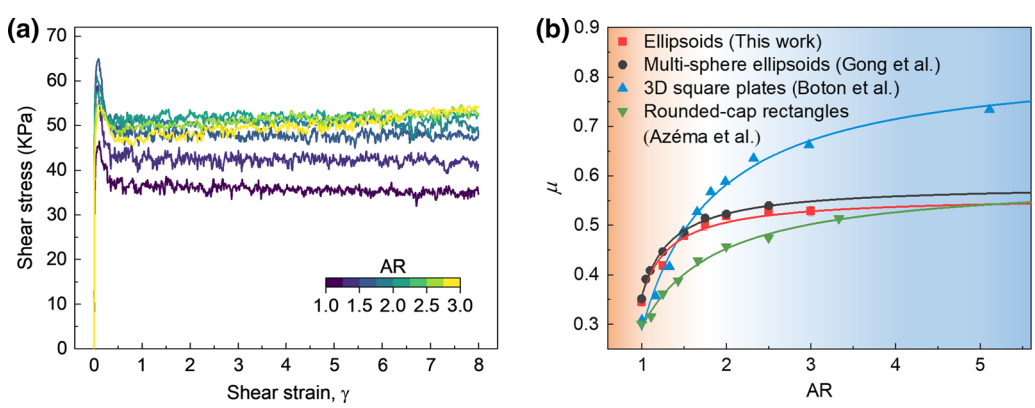

Fig. 3 **a** Stress–strain curves of granular systems with different particle shapes. The lines are colored based on particle AR. **b** Shear strength at steady state as a function of particle AR

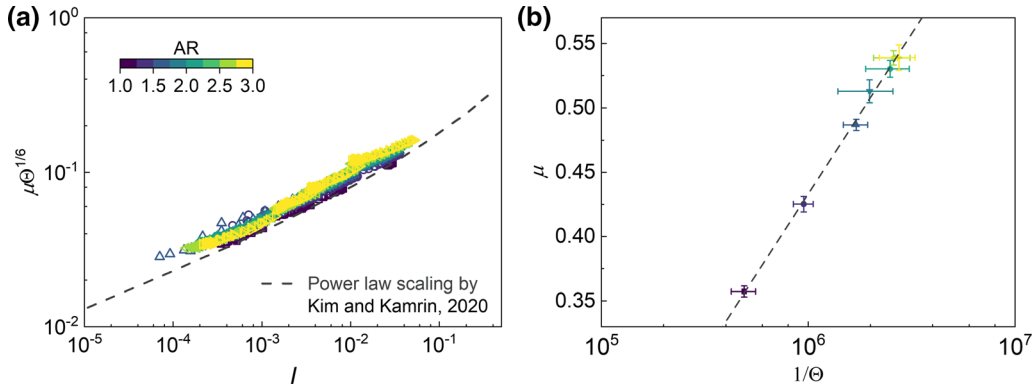

Fig. 4 **a** The relations between μ, I, and Θ in various granular layers. The dashed line is fit to the data of Kim and Kamrin [35]. **b** The relationship between μ and $1/\Theta$ of granular systems with different particle shapes. The dashed line is a logarithmic fit to the data. The data points in (**a, b**) are colored according to particle AR

local granular temperature T_{loc} of each particle is calculated as:

$$T_{\text{loc}} = \frac{1}{3N_i}\sum_{i}^{N_i}|\mathbf{v}_i - \overline{\mathbf{v}}|^2 \tag{5}$$

$$\overline{\mathbf{v}} = \sum_{j}^{N_i}\mathbf{v}_j V_j / \sum_{j}^{N_i} V_j \tag{6}$$

where $\mathbf{v}_i$ is the velocity of the particle i, and the index j iterates over the N_i neighbors of particle i. Two particles are defined to be neighbors if their Voronoi cells have a common face.

It should be noted that local granular temperature is a measure of the fluctuating (nonaffine) velocity of the particle, which is different from the temperature in thermodynamics. Recently, some scholars have also attempted to introduce rotational motion into the definition of local granular temperature [37]. Figure 5a shows the probability distribution functions of local granular temperature for granular systems with different particle shapes. The local granular temperature spans over several orders of magnitude, and its distribution is extremely nonuniform, exhibiting a power-law decay at the tail part. The 5% highest T_{loc} accounts for over half of the sum of granular temperature, suggesting that these particles mainly contribute to the granular temperature of the system. We take the particles with the top 5% local granular temperature as "active". Previous studies have shown that active particles tend to form compact clusters [11, 24, 46, 57]. We then identify those active clusters by connecting active particles that are neighbors. To avoid the unreasonable identification of the clusters, such as the case shown in Fig. 5b, in which two groups of particles connected by a single particle (colored gray) is identified as a cluster, we use the density-based spatial clustering of applications with noise (DBSCAN) clustering algorithm to identify active clusters [18].

In DBSCAN clustering, particles are classified as core particles, boundary particles, and outliers (Fig. 5c). One particle is regarded as a core particle (colored red) if the number of its neighbors is larger than the threshold (set to 3 in this study). The non-core particles with neighbors are defined as boundary particles (colored in yellow), whereas the particles without neighbors are taken as outliers (colored green). Each core particle is connected with its adjacent core particles and boundary particles to form clusters (marked by red dashed circles). Moreover, several adjacent boundary particles can form a small cluster without core particles (marked by a yellow dashed circle). Figure 5d, e shows typical snapshots of the active clusters formed in the granular systems with particle AR = 1.0 and 2.0, respectively. The active clusters demonstrate obvious differences in the cluster size and spatial distribution. Compared with spherical particles (Fig. 5d), the ellipsoidal particles tend to form larger active clusters and these clusters are concentrated in a more localized zone of the particle assembly (Fig. 5e).

We qualitatively characterize the active clusters, including the cluster size, cluster geometry, and spatial correlation. The cluster size s is defined as the number of particles in the cluster. The radius of gyration R_g of a cluster is calculated as:

$$R_g^2 = \frac{\sum_{i=1}^{s} V_i(\mathbf{r}_i - \overline{\mathbf{R}})}{\sum_{i=1}^{s} V_i} \tag{7}$$

where the summation is over s particles belonging to the cluster; V_i and $\mathbf{r}_i$ is, respectively, the volume and position of particle i; $\overline{\mathbf{R}}$ is the center of mass of the cluster calculated by $\overline{\mathbf{R}} = \sum_{i=1}^{N} V_i\mathbf{r}_i / \sum_{i=1}^{N} V_i$.

Figure 6a shows the cluster size distribution for a granular system with different particle shapes. The cluster

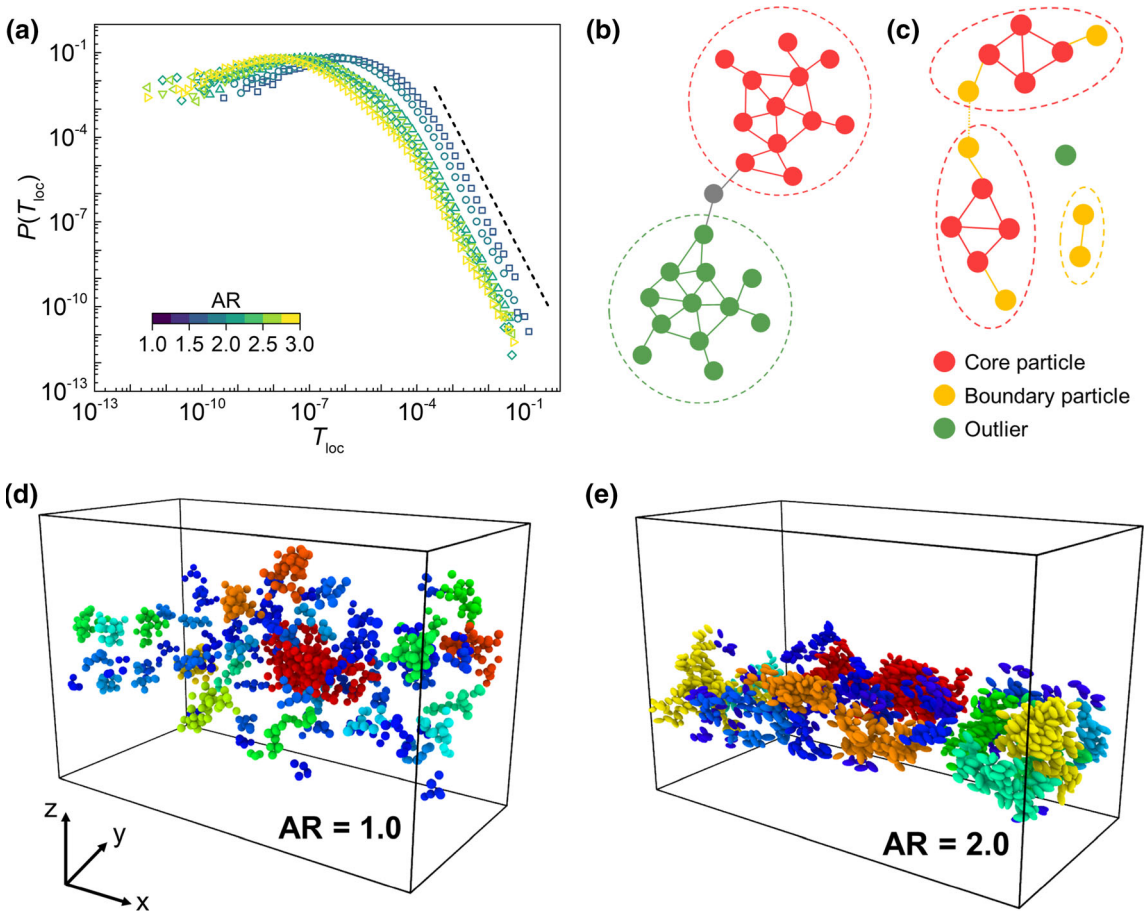

Fig. 5 **a** Probability distribution functions of local granular temperature for granular systems with different particle shapes. The dashed line is a guide to the eye. **b** Schematic illustration of the nonrealistic clustering by directly connecting active particles that are neighbors. **c** Schematic illustration of DBSCAN. **d, e** Snapshots of active clusters formed in granular systems with particle AR = 1.0 (**d**) and AR = 2.0 (**e**). For the sake of clarity, clusters with less than 4 particles are not shown

size shows a power-law decay distribution as $P(s) \sim s^{-\eta}$. As shown in Fig. 6b, the gyration radius shows a power-law growth with the cluster size, i.e., $R_g \propto s^{1/D}$, indicating that the clusters have fractal structures. Uncertainty of the fitting parameters was estimated using the bootstrap method. We resampled the cluster data 1000 times and then fitted the resampled data. The shape dependence of exponent η and fractal dimension D is shown in Fig. 6c. Both η and D decrease with increasing particle AR, indicating that aspherical particles tend to form active clusters of larger size and more anisotropy in shape. These results suggest that the spatial characteristic of microscopic plasticity is tuned by the particle shape, which may be the underlying mechanism responsible for the particle shape dependence of shear strength.

The emergence of active clusters implies that particle motion is collective. The different characteristics of active clusters give evidence to the different collective behaviors of granular systems with different particle shapes. To measure how far the granular temperature extends in space, we compute the characteristic length scale of active regions. The characteristic length is calculated according to $\xi^2 = 2\sum_i R_{gi}^2 s_i^2 / \sum_i s_i^2$, where R_{gi} is the radius of gyration for cluster size s_i [24]. Figure 7 shows the variations of characteristic length of active regions and its components in three directions with particle AR. Unlike the thermal systems, where the spatial correlations of microscopic fluctuations decay isotropically, the decay becomes directional dependent in the stress-driven granular materials. The characteristic length is longer in the shear direction (x-dir) and shorter in other directions [13]. The anisotropy of spatial correlations is more evident for aspherical particle assemblies, as confirmed by the ever-larger difference between ξ_x and ξ_y with the increasing particle AR. The characteristic length and its component in the shear direction increase with particle AR and saturate as AR $\geq$ 2.0. The variation of characteristic length of active regions with particle AR is consistent with the asymptotic convergence of shear strength. Moreover, our previous study has shown that the change in the stress state during

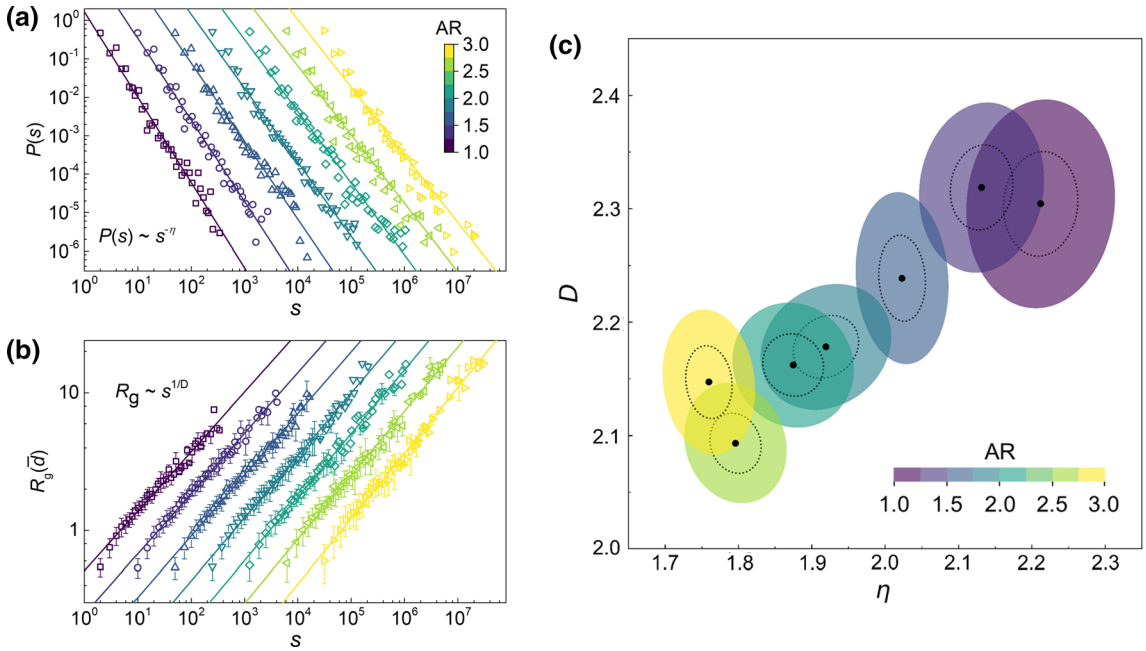

Fig. 6 **a, b** Cluster size distributions (**a**) and radius of gyration of the active cluster versus cluster size (**b**) for granular systems with different particle ARs. Data for AR ≥ 1.25 are shifted horizontally (by 5^1, 5^2, 5^3, 5^4, 5^5 and 5^6) for clarity. The solid lines are power-law fits to the data. **c** Parameter space for the power-law fits to $P(s)$ and R_g (s). The dotted (solid) ellipses around each best fit (η, D) are the 1σ (2σ) confidence regions as determined by the bootstrap method

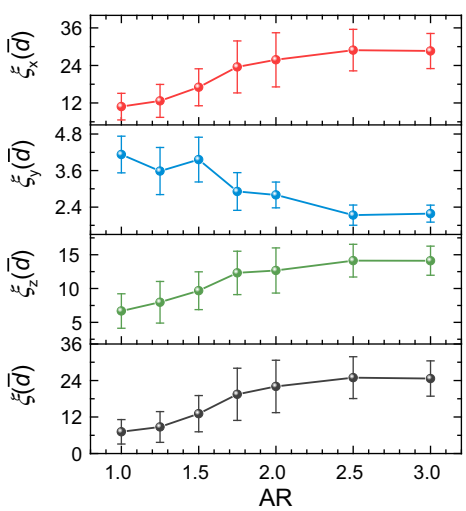

Fig. 7 Relations between characteristic length of active regions and its components in three directions with particle AR

shearing corresponds to the evolution of active region inside which the particles undergo nonaffine rearrangement [43]. Once the stress ratio reaches the steady state, the active region will remain stable for the remainder of loading. The rearrangement of particles may be the key to understanding the dynamic origin of shear strength. The larger characteristic length implies more collective motions, which is responsible for the increasing viscosity of dense suspensions [61]. Similarly, granular materials with more intensive collective motions can mobilize higher resistance to shear deformation.

4 Coupling between translational and rotational dynamics

Recent experimental tests have revealed the complex coupling between translational and rotational particle dynamics [39], which may be the key to understand the higher granular temperature and larger characteristic length of active regions in granular materials made of irregularly shaped particles. Many previous studies attributed the increase of shear strength with particle shape irregularity to the enhancement of particle rolling resistance [34, 62, 72, 75, 76]. Several contact models with rolling resistance have been proposed and implemented in DEM code [1, 29, 31, 64]. Although the rolling resistance contact models have been widely used in DEM studies to consider the particle inter-locking effects [19, 56, 66], Zhao et al. [71] recently pointed out that the rolling resistance models have limitations in considering irregular particle shapes. Similar results have been found by the authors [79]. These studies highlight the key role of rotational dynamics in unveiling the effects of particle shape on shear strength.

Particle rearrangements and the resulting velocity fluctuations are often accompanied by particle sliding and rolling [63]. Figure 8 shows the evolutions of mean particle

angular velocity and the fraction of sliding contacts with particle AR. Sliding occurs when the tangential contact force exceeds its Coulomb limit. We can see that the fraction of sliding contacts increase and mean angular velocity decrease with the increasing particle AR, indicating that the particle motion changes from rolling dominated to sliding dominated as the particles become more irregular. Compared with particle rolling, contact sliding is a more 'expensive' process due to the frictional energy dissipation, leading to higher shear strength for non-spherical particle assemblies [10].

As the granular temperature and its spatial characteristics play an important role in the mobilization of shear resistance, we further explore the contributions of particle rolling and sliding to the granular temperature. Figure 9a shows a typical snapshot and the vertical profile of local granular temperature of the granular system with particle AR = 1.5. Particles with higher granular temperature are clustered along the shear direction and form a system spanning band-like region. Figure 9b shows the vertical profiles of angular velocity and the number of sliding contacts. Local granular temperature correlates well with the particle angular velocity. However, the sliding contacts show no apparent correlation with the local granular temperature. The correlation analysis indicates that the particle rotational dynamic has a more direct relation with particle rearrangement. Figure 9c–d shows typical snapshots of fast transition particles and fast rotating particles (green and blue, respectively) for granular systems with particle AR = 1.0 and AR = 2.0. The fast translation particles are defined as those with 5% highest local granular temperature. The fast rotation particles are defined as those with 5% highest angular velocity. A significant part of the fast translating particles is also fast rotating (colored in red), providing direct evidence that the rotational and translational motion are significantly coupled. This analysis again

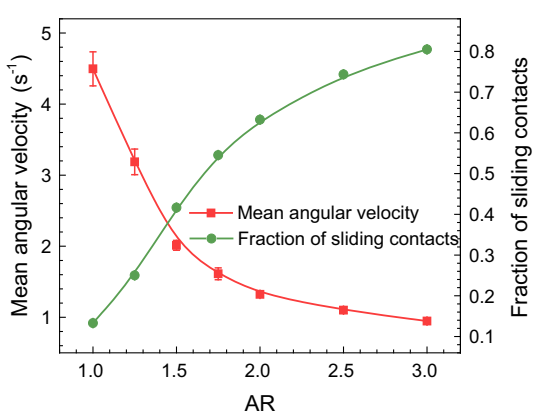

Fig. 8 Variations of mean particle angular velocity (red line) and the fraction of sliding contacts (green line) with particle AR (color figure online)

demonstrates that the granular temperature is significantly affected by particle rolling rather than sliding. However, this does not mean that particle sliding does not influence granular temperature and shear strength. In what follows, we will illustrate that particle sliding influences the shear strength by regulating the rotational behavior.

We have noticed that particle rolling has a significant influence on granular temperature. To measure how far the particle rotational dynamics extends in space, we calculate the spatial correlation function of particle angular velocity $C_\omega(\Delta r) = \left(\langle\omega(r+\Delta r)\omega(r)\rangle - \langle\omega(r)\rangle^2\right)/\left(\langle\omega^2(r)\rangle - \langle\omega(r)\rangle^2\right)$, which correlates angular velocity ω at locations separated by Δr. As shown in Fig. 10a, the correlations decay exponentially with the distance between particles, which can be fitted by an exponential function $C_\omega(\Delta r) \sim \exp(-\Delta r/\xi_r)$, where ξ_r is the correlation length [61]. The correlation length ξ_r as a function of particle AR is shown in the inset. The correlation length characterizing the internal scaling relation of particle rolling grows with particle AR, and it saturates at AR $\geq$ 2.0. Imagining a rotating particle as a point source perturbation, particles with much more irregular shapes are able to affect the particles far away from the rolling site due to the interlocking effects. From another point of view, the rotation of particles with more irregular shapes will be blocked by more particles, resulting in higher rolling resistance. Therefore, the correlation length of angular velocity can be considered a measure of rolling resistance. The relationship between the correlation length and particle shape also explains why using the rolling resistance model can reproduce the main macroscale mechanical behavior of non-spherical particles.

Figure 10b presents a strong relationship between the correlation length of particle angular velocity and the stress ratio at steady state. The property at the assembly level is directly related to the spatial length scale of particle dynamics. Moreover, both the correlation length and shear strength saturate at AR $\geq$ 2.0. Combing the analysis above, we can reach the conclusion that the shear strength of granular materials is controlled by the characteristic length of active regions and the correlation length of particle rotational dynamics. As strong coupling exists between the translational and rotational particle dynamics, these two length scales are essentially related to each other. The clear relationship between shear strength and the intrinsic length scale may provide a more general understanding of the linkage between macroscopic responses and microscopic dynamics of granular materials.

Similar to the relationship between shear strength and particle asphericity observed herein, previous studies have found that the shear strength of granular materials first

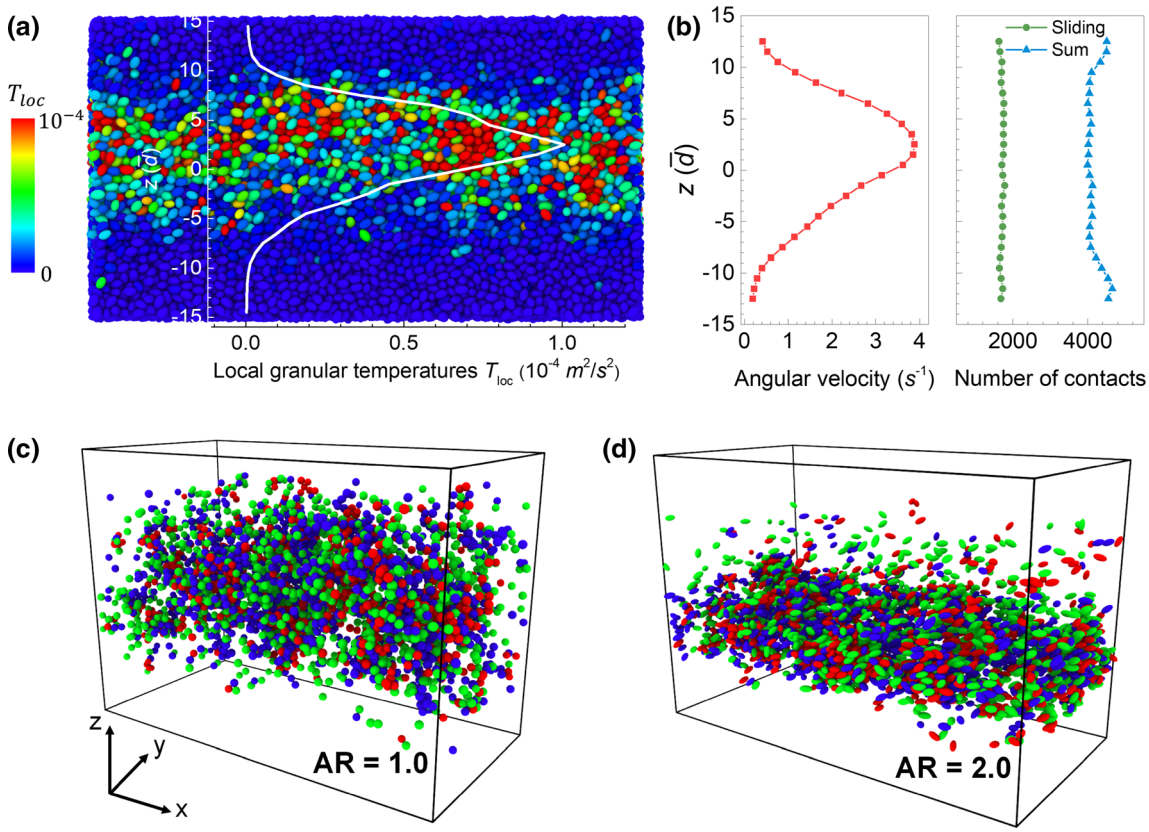

Fig. 9 **a** Spatial map of the local granular temperature of the granular system with particle AR = 1.5. The white line is the vertical profile of local granular temperature. **b** Profiles of angular velocity and the number of sliding contacts along the system height. **c, d** Snapshots showing the fast translating (green) and fast rotational (blue) particles. Also shown are the particles that are fast translating as well as fast rotating (red). **c, d** For granular systems with particle AR = 1.0 and AR = 2.0, respectively (color figure online)

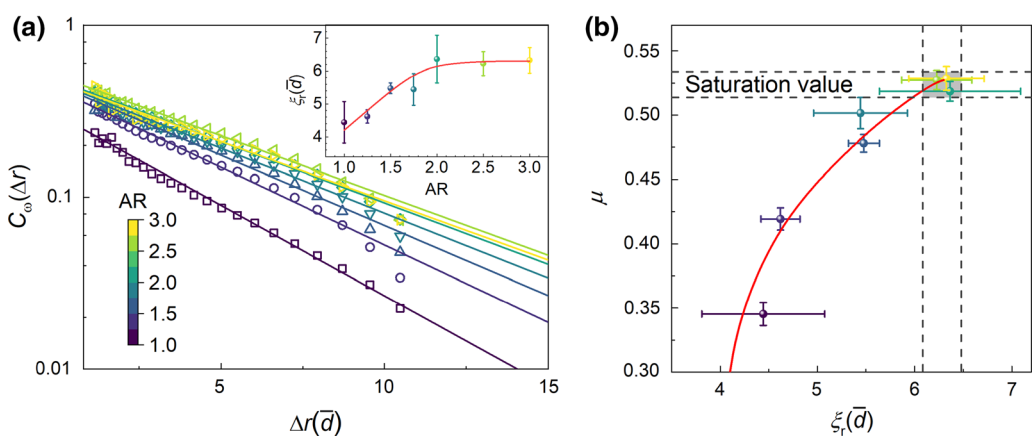

Fig. 10 **a** Spatial correlations of particle angular velocity for granular systems with different particle shapes. Δr is in units of the mean particle diameter. Solid lines are fits to an exponential function. The inset shows angular velocity correlation length as a function of particle AR, in which the red line is a guide to the eye. **b** Monotonic growth of shear strength with the correlation length of angular velocity. The red line is also a guide to the eye. The data points in both subplots are colored according to particle AR

increases with interparticle friction and then reaches a plateau at large interparticle friction [15, 17, 27, 70]. Dorostkar and Carmeliet [17] attributed this phenomenon to the fact that particle dynamics showing a transition from sliding to rolling due to the increase of interparticle friction. Recalling the transition of particle dynamics from rolling to sliding with increasing particle asphericity, we believe there is a negative feedback mechanism between the rotational and translational particle dynamics. In dense granular systems, the collective motion propagates in space

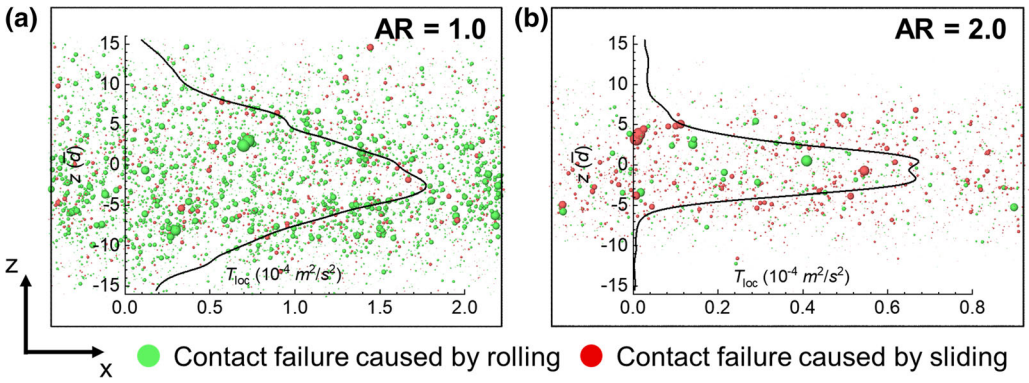

Fig. 11 **a, b** Spatial distribution of two types of contact failures for granular systems with AR = 1.0 (**a**) and AR = 2.0 (**b**). The size and color of spheres indicate the magnitude and type of failure contact, respectively. The black lines are the vertical profiles of local granular temperature (color figure online)

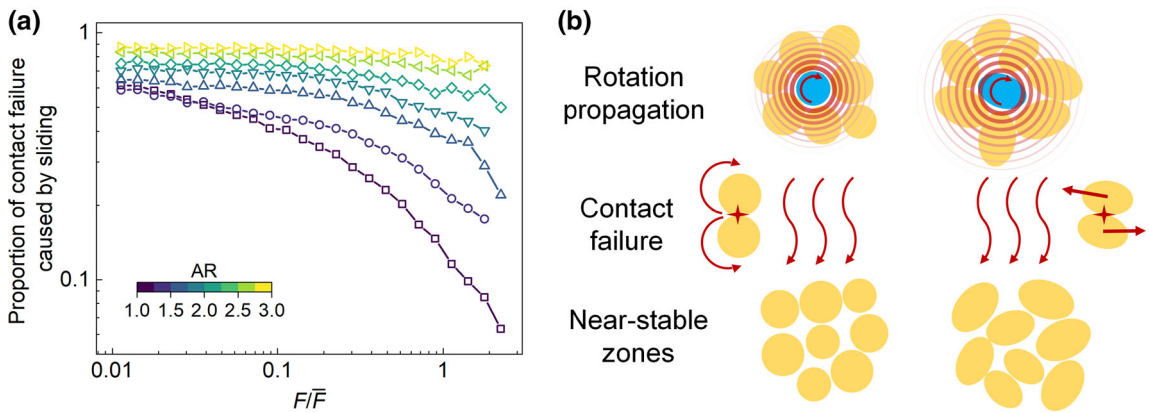

Fig. 12 **a** Relations between the proportion of contact failure caused by sliding and normalized contact force for granular systems with different particle shapes. **b** Picture illustrating the mechanism of long-range dynamic correlations

through particle contacts. Meanwhile, the contact failure caused by particle rolling and sliding will suppress this long-range behavior. It eventually leads to the spatial correlation of rotational dynamics decaying exponentially in space and disappearing till the induced disturbance is not able to overcome the rolling resistance. Figure 11a, b shows the snapshots of two types of contact failure that occur within the strain interval of $\Delta\gamma = 1.0\%$ for granular systems with particle AR = 1.0 and 2.0, respectively. The size and color of spheres denote the magnitude and type of contact failure. The black lines are the vertical profiles of local granular temperature. We find the failures of strong contacts most occur in the zone with high granular temperature, showing a strong correlation between force chain instability and particle nonaffine rearrangement. Moreover, for spherical particle assembly, there are significant number of separated contacts and most of them are caused by rolling (green). In contrast, the contact failure caused by sliding (red) take the majority in ellipsoidal particle assembly.

Figure 12a shows the relations between the proportion of contact failures caused by sliding and normalized contact force. For spherical particle assembly, the majority of sliding contacts are weak contacts ($F/\overline{F} < 1$). While for non-spherical particle assemblies, the fraction of contact failures caused by sliding increases, and many strong contacts ($F/\overline{F} > 1$) also fail by sliding. Based on the analysis above, we propose a physical picture of the particle shape effects on long-range dynamic correlations. As shown in Fig. 12b, the contact failure due to particle rolling suppresses the long-range propagation of particle dynamics in spherical particle assembly. While for non-spherical particle assemblies, the inter-locking effects enhance the long-range correlations of particle dynamics, but the contact sliding could also prohibit the particle dynamics from extending further.

5 Conclusions

In this work, we presented a microscopic investigation of the effects of particle shape on the shear strength of granular materials. To the best of our knowledge, this is the

first time that the particle shape dependence of shear strength is investigated from the perspective of particle dynamics. We confirmed that the power-law scaling in nonlocal granular rheology remains valid for non-spherical granular assemblies. The universal scaling between macroscopic stress ratio and granular temperature thus provides an informative clue to decoding the long-standing mystery concerning the nonlinear increase of shear strength with particle asphericity and saturates when particles become more irregular.

The particles with higher granular temperature tend to gyrate together and form clusters, showing dynamical heterogeneity. Compared with spherical particles, non-spherical particles tend to form active clusters of larger size and more anisotropy in shape, indicating the different spatial correlation patterns. Both the characteristic length of active regions and spatial correlation length of particle angular velocity increase with particle AR and saturate at AR $\geq$ 2.0, which coincides with the growth of shear strength. These two length scales are essentially related to each other because a strong coupling exists between the translational and rotational particle dynamics. Therefore, the macroscopic shear strength shows a clear relationship with the intrinsic length scale reflecting long-range dynamic correlations.

Based on the above observations, we have further proposed a physical picture of the particle shape effects on long-range dynamic correlations. In the conventional scenario, the effect of particle shape on granular materials is mainly attributed to the inter-locking effects. The collective particle motions and their long-range correlations provide a more fundamental explanation for the effect of particle shape. With the increase of particle asphericity, the contact failures experience a transition from rolling dominated to sliding dominated. The saturation of shear strength at a large AR is attributed to the fact that contact sliding suppresses the propagation of rotational particle dynamics, which finally leads to the nonlinear increase and saturation of shear strength.

Acknowledgements We acknowledge the financial support from the National Natural Science Foundation of China (Grant Nos. 51825905 and U1865204) and Science project of China Huaneng Group Co. Ltd (HNKJ18-H26). JZ acknowledges the support of MOE Chang Jiang Scholars Scheme. The numerical calculations in this work have been done on the supercomputing system in the Supercomputing Center of Wuhan University.

References

1. Ai J, Chen J, Rotter JM, Ooi JY (2011) Assessment of rolling resistance models in discrete element simulations. Powder Technol 206:269–282. https://doi.org/10.1016/j.powtec.2010.09.030
2. Alshibli KA, Asce M, Cil MB (2018) Influence of particle morphology on the friction and dilatancy of sand. J Geotech Geoenviron Eng 144:04017118. https://doi.org/10.1061/(ASCE)GT.1943-5606.0001841
3. Arda C, Cinicioglu O (2021) Influence of grain shape on stress-dilatancy parameters. Granul Matter 23:1–19. https://doi.org/10.1007/s10035-021-01098-2
4. Azéma E, Estrada N, Radjaï F (2012) Nonlinear effects of particle shape angularity in sheared granular media. Phys Rev E Stat Nonlinear Soft Matter Phys 86:041301. https://doi.org/10.1103/PhysRevE.86.041301
5. Azéma E, Radjaï F (2010) Stress-strain behavior and geometrical properties of packings of elongated particles. Phys Rev E Stat Nonlinear Soft Matter Phys 81:051304. https://doi.org/10.1103/PhysRevE.81.051304
6. Azéma E, Radjaï F, Peyroux R, Saussine G (2007) Force transmission in a packing of pentagonal particles. Phys Rev E Stat Nonlinear Soft Matter Phys 76:011301. https://doi.org/10.1103/PhysRevE.76.011301
7. Barrett PJ (1980) The shape of rock particles, a critical review. Sedimentology 27:291–303. https://doi.org/10.1111/j.1365-3091.1980.tb01179.x
8. Binaree T, Azéma E, Estrada N et al (2020) Combined effects of contact friction and particle shape on strength properties and microstructure of sheared granular media. Phys Rev E 102:22901. https://doi.org/10.1103/PhysRevE.102.022901
9. Blodgett ME, Egami T, Nussinov Z, Kelton KF (2015) Proposal for universality in the viscosity of metallic liquids. Sci Rep 5:13837. https://doi.org/10.1038/srep13837
10. Boton M, Azéma E, Estrada N et al (2013) Quasistatic rheology and microstructural description of sheared granular materials composed of platy particles. Phys Rev E Stat Nonlinear Soft Matter Phys 87:032206. https://doi.org/10.1103/PhysRevE.87.032206
11. Chen Y, Ma G, Zhou W et al (2021) An enhanced tool for probing the microscopic behavior of granular materials based on X-ray micro-CT and FDEM. Comput Geotech 132:103974. https://doi.org/10.1016/j.compgeo.2020.103974
12. Chen H, Zhao S, Zhao J, Zhou X (2021) The microscopic origin of K0 on granular soils: the role of particle shape. Acta Geotech 16:2089–2109. https://doi.org/10.1007/s11440-021-01161-5
13. Chikkadi V, Mandal S, Nienhuis B et al (2012) Shear-induced anisotropic decay of correlations in hard-sphere colloidal glasses. EPL. https://doi.org/10.1209/0295-5075/100/56001
14. Cho G-C, Dodds J, Santamarina JC (2006) Particle shape effects on packing density, stiffness, and strength: natural and crushed sands. J Geotech Geoenviron Eng 132:591–602. https://doi.org/10.1061/(asce)1090-0241(2006)132:5(591)
15. Dai BB, Yang J, Zhou CY (2016) Observed effects of interparticle friction and particle size on shear behavior of granular materials. Int J Geomech 16:04015011. https://doi.org/10.1061/(asce)gm.1943-5622.0000520
16. Donev A, Cisse I, Sachs D et al (2004) Improving the density of jammed disordered packings using ellipsoids. Science (80-) 303:990–993. https://doi.org/10.1126/science.1093010
17. Dorostkar O, Carmeliet J (2019) Grain friction controls characteristics of seismic cycle in faults with granular gouge. J Geophys Res Solid Earth 124:6475–6489. https://doi.org/10.1029/2019JB017374
18. Ester M, Kriegel H-P, Sander J, Xu X (1996) A Density-Based Algorithm for Discovering Clusters in Large Spatial Databases with Noise. In: Proceedings of the 2nd International Conference on Knowledge Discovery and Data Mining. Portland, OR, USA, pp 226–231
19. Estrada N, Azéma E, Radjai F, Taboada A (2011) Identification of rolling resistance as a shape parameter in sheared granular

media. Phys Rev E Stat Nonlinear Soft Matter Phys 84:011306. https://doi.org/10.1103/PhysRevE.84.011306
20. Estrada N, Taboada A, Radjaï F (2008) Shear strength and force transmission in granular media with rolling resistance. Phys Rev E Stat Nonlinear Soft Matter Phys 78:1–11. https://doi.org/10.1103/PhysRevE.78.021301
21. Ferdowsi B, Griffa M, Guyer RA et al (2015) Acoustically induced slip in sheared granular layers: application to dynamic earthquake triggering. Geophys Res Lett 42:9750–9757. https://doi.org/10.1002/2015GL066096.A
22. Frenning G (2008) An efficient finite/discrete element procedure for simulating compression of 3D particle assemblies. Comput Methods Appl Mech Eng 197:4266–4272. https://doi.org/10.1016/j.cma.2008.05.002
23. Gaume J, Chambon G, Naaim M (2020) Microscopic origin of nonlocal rheology in dense granular materials. Phys Rev Lett 125:188001. https://doi.org/10.1103/PhysRevLett.125.188001
24. Ghosh A, Budrikis Z, Chikkadi V et al (2017) Direct observation of percolation in the yielding transition of colloidal glasses. Phys Rev Lett 118:148001. https://doi.org/10.1103/PhysRevLett.118.148001
25. Göncü F, Luding S (2013) Effect of particle friction and polydispersity on the macroscopic stress-strain relations of granular materials. Acta Geotech 8:629–643. https://doi.org/10.1007/s11440-013-0258-z
26. Gong J, Liu J (2017) Effect of aspect ratio on triaxial compression of multi-sphere ellipsoid assemblies simulated using a discrete element method. Particuology 32:49–62. https://doi.org/10.1016/j.partic.2016.07.007
27. Gong J, Zou J, Zhao L et al (2019) New insights into the effect of interparticle friction on the critical state friction angle of granular materials. Comput Geotech 113:103105. https://doi.org/10.1016/j.compgeo.2019.103105
28. Gonzalez M, Cuitiño AM (2016) Microstructure evolution of compressible granular systems under large deformations. J Mech Phys Solids 93:44–56. https://doi.org/10.1016/j.jmps.2016.03.024
29. Iwashita K, Oda M (1998) Rolling resistance at contacts in simulation of shear band. ASCE 124:285–292
30. Jaeger HM, Nagel SR, Behringer RP (1996) Granular solids, liquids, and gases. Rev Mod Phys 68:1259–1273. https://doi.org/10.1103/RevModPhys.68.1259
31. Jiang MJ, Yu HS, Harris D (2005) A novel discrete model for granular material incorporating rolling resistance. Comput Geotech 32:340–357. https://doi.org/10.1016/j.compgeo.2005.05.001
32. Johnson K (1985) Contact mechanics. UK Cambridge University Press, London
33. Kamrin K, Koval G (2012) Nonlocal constitutive relation for steady granular flow. Phys Rev Lett 108:178301. https://doi.org/10.1103/PhysRevLett.108.178301
34. Kandasami RK, Murthy TG (2017) Manifestation of particle morphology on the mechanical behaviour of granular ensembles. Granul Matter 19:1–13. https://doi.org/10.1007/s10035-017-0703-z
35. Kim S, Kamrin K (2020) Power-law scaling in granular rheology across flow geometries. Phys Rev Lett 125:88002. https://doi.org/10.1103/PhysRevLett.125.088002
36. Kloss C, Goniva C, Hager A et al (2012) Models, algorithms and validation for opensource DEM and CFD-DEM. Prog Comput Fluid Dyn 12:140–152. https://doi.org/10.1504/PCFD.2012.047457
37. Kong Y, Zhao J, Li X (2021) Hydrodynamic dead zone in multiphase geophysical flows impacting a rigid obstacle. Powder Technol 386:335–349. https://doi.org/10.1016/j.powtec.2021.03.053
38. Kou B, Cao Y, Li J et al (2017) Granular materials flow like complex fluids. Nature 551:360–363. https://doi.org/10.1038/nature24062
39. Kou B, Cao Y, Li J et al (2018) Translational and rotational dynamical heterogeneities in granular systems. Phys Rev Lett 121:018002. https://doi.org/10.1103/PhysRevLett.121.018002
40. Lashkari A, Falsafizadeh SR, Shourijeh PT, Alipour MJ (2020) Instability of loose sand in constant volume direct simple shear tests in relation to particle shape. Acta Geotech 15:2507–2527. https://doi.org/10.1007/s11440-019-00909-4
41. Ma G, Chen Y, Yao F et al (2019) Evolution of particle size and shape towards a steady state: Insights from FDEM simulations of crushable granular materials. Comput Geotech 112:147–158. https://doi.org/10.1016/j.compgeo.2019.04.022
42. Ma G, Regueiro RA, Zhou W et al (2018) Role of particle crushing on particle kinematics and shear banding in granular materials. Acta Geotech 13:601–618. https://doi.org/10.1007/s11440-017-0621-6
43. Ma G, Regueiro RA, Zhou W, Liu J (2019) Spatiotemporal analysis of strain localization in dense granular materials. Acta Geotech 14:973–990. https://doi.org/10.1007/s11440-018-0685-y
44. Ma G, Zhou W, Chang XL et al (2016) Formation of shear bands in crushable and irregularly shaped granular materials and the associated microstructural evolution. Powder Technol 301:118–130. https://doi.org/10.1016/j.powtec.2016.05.068
45. Ma G, Zhou W, Regueiro RA et al (2017) Modeling the fragmentation of rock grains using computed tomography and combined FDEM. Powder Technol 308:388–397. https://doi.org/10.1016/j.powtec.2016.11.046
46. Ma G, Zou Y, Chen Y et al (2021) Spatial correlation and temporal evolution of plastic heterogeneity in sheared granular materials. Powder Technol 378:263–273. https://doi.org/10.1016/j.powtec.2020.09.053
47. Ma G, Zou Y, Gao K et al (2020) Size polydispersity tunes slip avalanches of granular gouge geophysical research letters. Geophys Res Lett. https://doi.org/10.1029/2020GL090458
48. Midi GDR (2004) On dense granular flows. Eur Phys J E 14:341–365. https://doi.org/10.1140/epje/i2003-10153-0
49. Molina SL, Azema E, Estrada N et al (2019) Impact of grading on steady-state strength. Geotech Lett 9:328–333. https://doi.org/10.1680/jgele.18.00216
50. Murphy KA, Dahmen KA, Jaeger HM (2019) Transforming mesoscale granular plasticity through particle shape. Phys Rev X 9:11014. https://doi.org/10.1103/PhysRevX.9.011014
51. Ng TT, Zhou W, Ma G, Chang XL (2018) Macroscopic and microscopic behaviors of binary mixtures of different particle shapes and particle sizes. Int J Solids Struct 135:74–84. https://doi.org/10.1016/j.ijsolstr.2017.11.011
52. Ouadfel H, Rothenburg L (2001) 'Stress–force–fabric' relationship for assemblies of ellipsoids. Mech Mater 33:201–221. https://doi.org/10.1016/S0167-6636(00)00057-0
53. Podlozhnyuk A, Pirker S, Kloss C (2017) Efficient implementation of superquadric particles in Discrete Element Method within an open-source framework. Comput Mech 4:101–118. https://doi.org/10.1007/s40571-016-0131-6
54. Qi F, de Richter SK, Jenny M, Peters B (2020) DEM simulation of dense granular flows in a vane shear cell: Kinematics and rheological laws. Powder Technol 366:722–735. https://doi.org/10.1016/j.powtec.2020.03.008
55. Rathbun AP, Renard F, Abe S (2013) Numerical investigation of the interplay between wall geometry and friction in granular fault gouge. J Geophys Res Solid Earth 118:878–896. https://doi.org/10.1002/jgrb.50106
56. Rorato R, Arroyo M, Gens A et al (2021) Image-based calibration of rolling resistance in discrete element models of sand. Comput

Geotech 131:103929. https://doi.org/10.1016/j.compgeo.2020.103929
57. Royall CP, Williams SR, Ohtsuka T, Tanaka H (2008) Direct observation of a local structural mechanism for dynamic arrest. Nat Mater 7:2–7. https://doi.org/10.1038/nmat2219
58. Saint-Cyr B, Delenne JY, Voivret C et al (2011) Rheology of granular materials composed of nonconvex particles. Phys Rev E Stat Nonlinear Soft Matter Phys 84:041302. https://doi.org/10.1103/PhysRevE.84.041302
59. Schaller FM, Neudecker M, Saadatfar M et al (2015) Local origin of global contact numbers in frictional ellipsoid packings. Phys Rev Lett 114:158001. https://doi.org/10.1103/PhysRevLett.114.158001
60. Shinohara K, Oida M, Golman B (2000) Effect of particle shape on angle of internal friction by triaxial compression test. Powder Technol 107:131–136. https://doi.org/10.1016/S0032-5910(99)00179-5
61. Singh A, Ness C, Seto R et al (2020) Shear thickening and jamming of dense suspensions: the "roll" of friction. Phys Rev Lett 124:248005. https://doi.org/10.1103/PhysRevLett.124.248005
62. Suh HS, Kim KY, Lee J, Yun TS (2017) Quantification of bulk form and angularity of particle with correlation of shear strength and packing density in sands. Eng Geol 220:256–265. https://doi.org/10.1016/j.enggeo.2017.02.015
63. Suiker ASJ, Fleck NA (2004) Frictional collapse of granular assemblies. J Appl Mech Trans ASME 71:350–358. https://doi.org/10.1115/1.1753266
64. Tordesillas A, Walsh DCS (2002) Incorporating rolling resistance and contact anisotropy in micromechanical models of granular media. Powder Technol 124:106–111. https://doi.org/10.1016/S0032-5910(01)00490-9
65. Wang D, Carmeliet J, Zhou W, Dorostkar O (2021) On the effect of grain fragmentation on frictional instabilities in faults with granular gouge. J Geophys Res Solid Earth. https://doi.org/10.1029/2020jb020510
66. Wensrich CM, Katterfeld A (2012) Rolling friction as a technique for modelling particle shape in DEM. Powder Technol 217:409–417. https://doi.org/10.1016/j.powtec.2011.10.057
67. Xiao Y, Long L, Matthew Evans T et al (2019) Effect of particle shape on stress-dilatancy responses of medium-dense sands. J Geotech Geoenviron Eng 145:04018105. https://doi.org/10.1061/(ASCE)GT.1943-5606.0001994
68. Xu WJ, Liu GY, Yang H (2020) Study on the mechanical behavior of sands using 3D discrete element method with realistic particle models. Acta Geotech 15:2813–2828. https://doi.org/10.1007/s11440-020-00982-0
69. Yang J, Luo XD (2015) Exploring the relationship between critical state and particle shape for granular materials. J Mech Phys Solids 84:196–213. https://doi.org/10.1016/j.jmps.2015.08.001
70. Yang SH, Zhou W, Ma G et al (2020) Mechanism of inter-particle friction effect on 3D mechanical response of granular materials. Yantu Gongcheng Xuebao Chin J Geotech Eng 42:1885–1893. https://doi.org/10.11779/CJGE202010014
71. Zhao S, Evans TM, Zhou X (2018) Shear-induced anisotropy of granular materials with rolling resistance and particle shape effects. Int J Solids Struct 150:268–281. https://doi.org/10.1016/j.ijsolstr.2018.06.024
72. Zhao J, Guo N (2014) Rotational resistance and shear-induced anisotropy in granular media. Acta Mech Solida Sin 27:1–14. https://doi.org/10.1016/S0894-9166(14)60012-4
73. Zhao S, Zhao J, Guo N (2020) Universality of internal structure characteristics in granular media under shear. Phys Rev E 101:12906. https://doi.org/10.1103/PhysRevE.101.012906
74. Zhao S, Zhou X (2017) Effects of particle asphericity on the macro- and micro-mechanical behaviors of granular assemblies. Granul Matter 19:1–18. https://doi.org/10.1007/s10035-017-0725-6
75. Zhou B, Huang R, Wang H, Wang J (2013) DEM investigation of particle anti-rotation effects on the micromechanical response of granular materials. Granul Matter 15:315–326. https://doi.org/10.1007/s10035-013-0409-9
76. Zhou W, Ma G, Chang X, Zhou C (2013) Influence of particle shape on behavior of rockfill using a three-dimensional deformable DEM. J Eng Mech 139:1868–1873. https://doi.org/10.1061/(ASCE)EM.1943-7889.0000604
77. Zhou Z, Wang H, Jiang M (2021) Macro- and micro-mechanical relationship of the anisotropic behaviour of a bonded ellipsoidal particle assembly in the elastic stage. Acta Geotech. https://doi.org/10.1007/s11440-021-01328-0
78. Zhou W, Wu W, Ma G et al (2018) Undrained behavior of binary granular mixtures with different fines contents. Powder Technol 340:139–153. https://doi.org/10.1016/j.powtec.2018.09.022
79. Zou YX, Ma G, Li YA et al (2020) Impact of rotation resistance on fabric of granular materials. Yantu Lixue/Rock Soil Mech 41:2829–2838. https://doi.org/10.16285/j.rsm.2019.1703

Publisher's Note Springer Nature remains neutral with regard to jurisdictional claims in published maps and institutional affiliations.